

Synthesis, structural and optical properties of Ag doped ZnO nanoparticles with enhanced photocatalytic properties by photo degradation of organic dyes

Rajender Singh^{1,2} · P. B. Barman¹ · Dheeraj Sharma¹

Received: 9 September 2016 / Accepted: 16 December 2016 / Published online: 9 January 2017
© Springer Science+Business Media New York 2017

Abstract In present paper chemical route based synthesis of Ag doped ZnO nanoparticles (NPs) by co-precipitation method is reported to develop ZnO NPs for photo catalytic application. XRD confirms the structural purity of ZnO NPs. FESEM and TEM study reveals the surface and ultra structure morphology of NPs. EDAX study confirms the purity and homogeneity of NPs. The Ag/ZnO NPs with different weight percentage of Ag relative to ZnO were applied under visible light irradiation for evaluating heterogeneous photo catalytic degradation of methylene blue (MB) and Brilliant blue (BB) respectively. The presence of Ag in ZnO enhance MB and BB dye degradation effectiveness from 96.78 to 98.66 and 82.15 to 97.36% for pure ZnO and maximum Ag doped ZnO ($x=0.1$) respectively. In comparison of MB and BB final degradation ability, MB dyes have more effective photo catalytic efficiency towards different oxidizing species to degradation process.

1 Introduction

The organic dyes originated from different sources such as textiles, dyeing, pharmaceutical, paper industry bring organic pollutants to natural water, make it contaminated. The toxicity and hazardous nature of different organic pollutants in fresh water resources bring severe environment and health problems. There are some physical and chemical processes such as ultra-filtration, reverse osmosis, adsorption, precipitation etc. applied to remove toxic substances from wastewater making it pure. These conventional techniques for purification of waste water in due time transform organic pollutants into other toxic substances [1]. Semiconductor based photocatalysts addresses problem of dyes removal from waste water very effectively. Therefore semiconductor based photocatalyst have attracted wide attention of researcher for problem of waste water purification.

Different semiconductors have been used as photo catalyst till now such as TiO_2 , ZnO, ZnS, WO_3 , CdS etc [2–6]. Among all, ZnO (Zinc oxide) is the best candidate for photo catalysis due to its high efficiency, photochemical stability and cost effectiveness. ZnO has importance as a industrial material because of its semiconducting and inorganic base that have structure as wurtzite [7]. Due to wide band gap (3.30 eV), large exciton binding energy (60 meV) of ZnO nanoparticles (NPs), their transparency to visible light and absorbing capacity in the UV-light, will makes it justified in water purification. In addition ZnO has many applications in field such as transparent electrodes [8], gas sensor [9], light emitting diode [10], laser system [11], photo catalytic processes [12, 13] etc. The pure ZnO may not give desirable photocatalytic result due to high optical band gap which do not absorb visible light, so dopants are used to tune optical band gap of ZnO to match its energy with visible light energy. Different dopants such as transition metal

✉ Rajender Singh
rajenderphysics@gmail.com

P. B. Barman
pb.barman@juit.ac.in

Dheeraj Sharma
dheeraj.sharma@juit.ac.in

¹ Department of Physics and Materials Science, Jaypee University of Information Technology, Wanknaghat, Solan 173234, Himachal Pradesh, India

² Department of Central Instrumentation Laboratory (CIL), Panjab University, Chandigarh, India

doping [14] or noble metal doping [15] can be the best option.

Doping with noble metals named as gold (Au), palladium (Pd), silver (Ag) etc. in ZnO have major effect on its photo-catalytic activity [16–18]. Silver (Ag) doping in ZnO can be the best candidate to achieve the desired properties by co-precipitation method [19, 20]. Reason to choose silver as dopant is due its ability to generate region of electric field and improved electrical properties by optical vibration of surface Plasmon [21]. Doping of Ag in ZnO matrix will lead to induce oxygen vacancies [15], crystal defects [22], higher light scattering [23] collectively contribute to the enhanced efficiency of photo catalytic activity of ZnO NPs.

The main objective of this study is to investigate cause for variable degradation abilities of Ag doped ZnO with different dye. In order to fulfill this requirement the quality ZnO nanoparticles have been produced for dye removal, to utilize their effective structural and morphological properties. It has been observed that the photo-catalytic activity of ZnO nanoparticles (NPs) is due to electron/hole (e^-/h^+) generation under illumination of light. More the separation of electron/hole (e^-/h^+), leads to higher probability of formation of superoxide radicals and holes which attack on organic compounds [24].

There are lot of studies performed on photocatalysis activity of Ag doped ZnO with different organic dyes (Methylene Blue, Brilliant blue, Methylene orange, Naphthol blue black, Rhodamine etc) [25–29], which still being carried out for need further exploration in their degradation mechanism. In present work we have carried out the comparative study of methylene blue (MB) and brilliant blue (BB) dyes degradation ability with Ag doped ZnO to find unexplored aspects of their heterogenous photocatalysis mechanism and to make a comparison study, which is rarely found.

MB and BB dyes are the representative of organic contaminants in waste water, so their removal from water could be one remedial alternative for water purification.

In this respect the synthesized ZnO NPs with Ag doping could be the best option among different material present in market for water purification and lead to make waste water useable for society.

2 Materials and methods

All chemicals used in the study (Zinc nitrate hexahydrate 99%, silver nitrate 99.8%, NaOH 98.56%) were AR grade purchased from HiMedia, Mumbai, India. All reagents were prepared by using deionized water.

2.1 Synthesis of $Zn_{1-x}Ag_xO$ ($x=0, 0.02, 0.04, 0.06, 0.1$) NPs

Ag doped ZnO NPs were synthesized by the co-precipitation method. Zinc nitrate hexa hydrate and silver nitrate were used as precursor to prepare their NPs. Known amount of Zinc nitrate hexa hydrate and silver nitrate dissolved in distilled water under magnetic stirring for 30 min to make a homogeneous solution. In above solution 0.5 M NaOH was added dropwise with continuous stirring. After complete addition of NaOH, the precipitated solution was left overnight and then decant the supernatant liquid carefully into whatman qualitative filter having pore size 20–25 μ without disturbing the precipitate. The precipitate was centrifuge at 5000 rpm and dried at 110 °C for overnight, grind and calcined at 500 °C for 3h. Finally ZnO NPs were obtained. Zinc oxide (ZnO) with different concentration of Ag ($X=0, 0.02, 0.04, 0.06, 0.1$) were synthesized named as ZnOAg0, ZnOAg1, ZnOAg2, ZnOAg3 and ZnOAg4 respectively. The Fig. 1 gives schematic representation of synthesis and its reaction mechanism respectively.

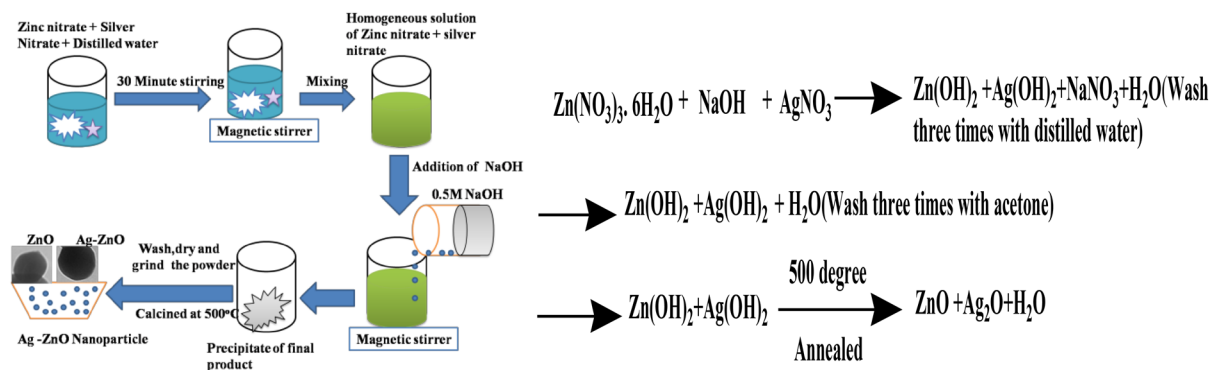


Fig. 1 Schematic representation of synthesis and its possible reaction mechanism respectively

2.2 Characterization methods

XRD was recorded with help of Panalytical make XPERT-PRO ($\lambda = 1.54060\text{\AA}$). The UV–visible (UV–Vis) absorption spectra of different samples were recorded using PerkinElmer Model Lamda 750. FESEM-EDAX images and spectrum were recorded by using Hitachi model SU8010. TEM images were taken with Hitachi H-7500 instrument with 120KV accelerating voltage. The photo catalytic reaction was performed under 500 W Halogen lamp as the source visible light (emission range ~400–800 nm).

3 Result and discussion

3.1 Structural properties

XRD peaks of pure ZnO were indexed by hexagonal wurtzite phase of ZnO (JCPDS Card No. 36-1451) shown in Fig. 2(left). Pure ZnO has peaks at 2θ value of 31.65° , 34.47° , 36.26° , 47.67° , 56.64° , 62.90° , 66.49° , 68.03° , 68.80° , 72.45° and 77.23° corresponding to diffraction of the (100), (002), (101), (102), (110), (103), (200), (112), (201), (004) and (202) planes respectively. The highly indexed ZnO peaks confirm the purity of ZnO phase and nonexistence of the impurities. Broadened peaks of pure

ZnO XRD pattern authenticate the formation of nanocrystals. As ZnO have wurtzite structure in which oxygen atoms are arranged in hexagonal closed packing with Zinc atom occupying half of tetrahedral sites. Zinc and oxygen atoms are tetrahedrally coordinated to each other so have an equivalent position. As we have doped the Ag phase ($X=0, 0.02, 0.04, 0.06, 0.1$) into the ZnO structure, we got Ag phase induced at angle 38.22 and 44.20° in ZnOAg3 ($X=0.06$) and ZnOAg4 ($X=0.1$) respectively. This suggests Ag as the secondary phase present in the ZnO matrix. The shifting in 101 peak positions can be due to difference in ionic radii of Ag^+ (1.26\AA) and Zn^{+2} (0.74\AA) respectively. Up to $X=0.04$ doping level of Ag, there is no Ag peak present in ZnO matrix directs its substitution mechanism whereas for $X=0.06$ and 0.1 , clear Ag peak in ZnO lattice predicts Ag position at interstitial site. Ag position at substitution or interstitial site in ZnO lattice can be ensured by measurable peak shift to lower [30] and higher [31] 2θ respectively. The same pattern was observed in Fig. 2(left) of peak shifting of 101 peak to lower angle upto $X=0.04$ in ZnO (substitution of silver) and peak shifted to higher angle for $X=0.06$ and 0.1 (Interstitial position of silver) respectively. The shifting of 101 diffraction peaks and change in Full width Half Maxima (FWHM (Table 1), indicates change in crystallinity of ZnO through doping of silver [32].

Fig. 2 Left The XRD pattern for pure ZnO NPs and Ag doped ZnO nanoparticles (ZnOAg0, ZnOAg1, ZnOAg2, ZnOAg3 and ZnOAg4) and right enlarged region XRD pattern from 36.0° to 36.6° (2θ) respectively

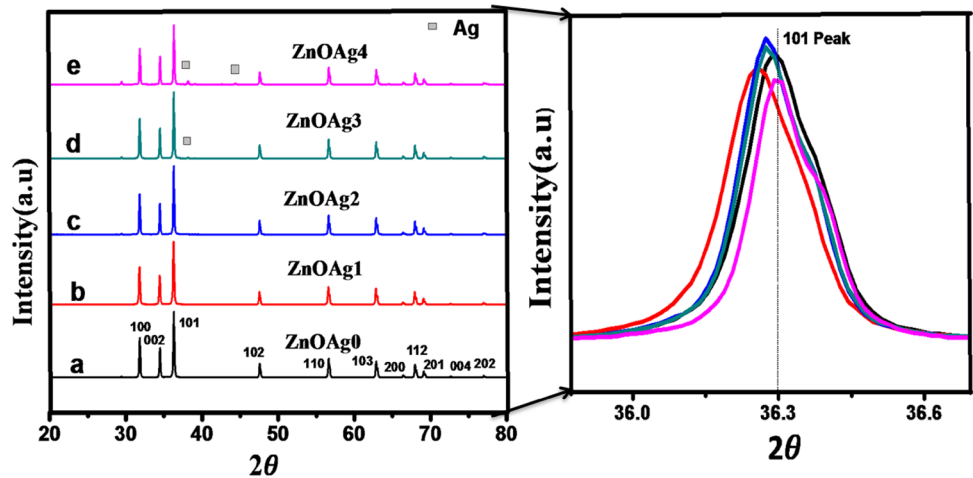


Table 1 Crystallite size, micro-strain, position and FWHM (101 peak) of Ag doped ZnO nanocomposite

S. No.	D (nm)	Strain ϵ (10^{-4})	Position of 101 peak with FWHM ($^\circ$)	Intensity ratio of 002 peak to 101 peak
ZnOAg0	46.47	23.90	36.26 (0.18)	0.4553
ZnOAg1	44.44	27.85	36.20 (0.21)	0.4750
ZnOAg2	49.59	22.57	36.22 (0.17)	0.4441
ZnOAg3	51.74	22.40	36.22 (0.16)	0.4461
ZnOAg4	54.80	22.36	36.25 (0.15)	0.4891

As ZnO crystallizes in wurtzite structure, the inter planner spacing of given Miller indices h, k, l , and d_{hkl} values of ZnO: Ag NPs were calculated by using Bragg's equation [33] as follows

$$2d \sin\theta_{hkl} = n\lambda \quad (1)$$

where n is the order of diffraction ($n=1$) and λ is X-ray wavelength.

3.2 Crystallite size and strain

The average crystallite size of pure ZnO and Ag doped ZnO nanocomposite calculated by Scherrer equation (2) [33] summarized in Table 1.

$$D = k\lambda / \beta_{hkl} \cos(\theta) \quad (2)$$

where β_{hkl} is full width half maximum of diffracting peak, k is constant equal to 0.90, λ is X-ray energy of incident source ($\lambda = 0.1540$ nm), D is crystallite size and θ is bragg angle respectively.

Micro strain (ϵ) for prepared NPs is calculated by using Eq. (3) [34],

$$\epsilon = \frac{\beta_{1/2}}{4 \tan(\theta)} \quad (3)$$

where is the full width at half maximum of (101) peak and (θ) is the bragg angle.

From Table 1, it has been found with Ag doping in pure ZnO, initially minor decrease in crystallite size to 44.44 nm from 46.47 and then increases to 49.59, 51.74 and 54.80 nm with increasing doping level of Ag from $x=0.02$ to 0.1. The micro strain increases with decrease in crystallite size and vice versa as mention in Table 1. With addition of Ag in ZnO, the shifting in position and change in FWHM value of 101 peak with respect to ZnOAg0 is observed, which indicates structural changes in Ag doped ZnO NPs with respect to pure ZnOAg0 as mentioned in Table 1. In addition to study the effect of silver in ZnO studied through intensity ratio of 002 peak to 101 peak of different samples was calculated and summarized in Table 1. The values of 002 peak to 101 peak intensity ratio are 0.4553, 0.4750, 0.4441, 0.4461 and 0.4891 for ZnOAg0, ZnOAg1, ZnOAg2, ZnOAg3 and ZnOAg4 respectively. From intensity ratio, the clear changes in intensity ratio with doping of silver is observed, which predict the alteration in ZnO structure through silver.

Figure 3 depict the change in values of crystallite size (D) and stain (ϵ) at different content of Ag in ZnO. All these alteration in structural parameters of Ag doped ZnO with reference to pristine ZnO, confirm the presence of Ag in ZnO matrix [34].

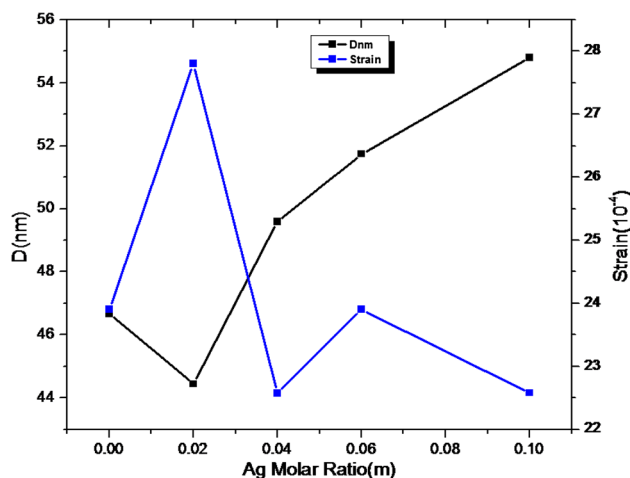


Fig. 3 Change in crystallite size and residual stress of un-doped and Ag doped ZnO NPs

3.3 Optical study

The Fig. 4(left) shows the absorption spectra as a function of wavelength for undoped and Ag doped ZnO NPs. The absorption spectra of pure ZnO (ZnOAg0) we got maximum absorption at 373.2 nm. Further with Ag addition $x=0.1$ (ZnOAg4), absorption edge shifted to higher wavelength (377 nm) with respect to pure ZnO. This shift in absorption edge may be attributed to incorporation of Ag in ZnO matrix. This will lead to narrowing the optical band gap with Ag doping in ZnO as shown in Fig. 4(2) [35] and values are summarized in Table 2. The decrease of optical band gap of ZnO with silver can be due to induced band gap renormalization effect [36]. The factor responsible for the renormalization of band gap is due to exchange interaction (sp-d) in band electrons and localized d-electrons of Ag^+ . After the possible exchange interaction, there will be modification in band gap of different Ag doped ZnO with reference to pure ZnO.

In case of direct band gap transition, optical band gap and absorption coefficient are correlated by Eq. 4 [10].

$$ah\nu = [A(h\nu - E_g)]^{(1/2)} \quad (4)$$

where A is constant, $h\nu$ is photon energy and E_g is optical band gap.

The optical band gap decreases from 3.13 to 2.75 eV for pure ZnO to ZnO with Ag, $x=0.1$ (ZnOAg4) respectively. The decrease in band gap with Ag doping in ZnO may be due to presence of oxygen vacancies which makes the path of electrons easy from valance band (VB) to conduction band (CB) [10]. The calculated values are summarized in Table 2. This may be correlated that when concentration of oxygen vacancies is increased, impurity states become

more delocalized and overlap with valance band edge of ZnO leads to decrease the final band gap. Collectively the overall decrease in band gap can be due to Ag content and oxygen vacancies incorporation in pure ZnO leads its visible absorption red shifted as shown in Fig. 4(1).

In addition the optical band gap can also be defined in terms of localized states, in which the absorption coefficient $\alpha(\omega)$ calculated through the Urbach formula as mention in Eq. 5 [37]

$$\alpha(\omega) = \alpha_0 \exp\left(\frac{\hbar\omega}{\Delta E}\right) \tag{5}$$

where α_0 constant and ΔE is energy which is correlated as width of localized states in forbidden band gap.

The reciprocal of slope of straight line of Eq. 5, will gives the values of ΔE . The calculated value of ΔE contributed to optical band gap (E_{opt}) of ZnO. The presence of localized states in band gap will lead to change the mobility gap. Higher the value of ΔE means higher localized states (defects) in material leading to more possibility in alteration in optical properties.

3.4 FESEM study

The FESEM images of synthesized ZnO NPs are shown in Fig. 5. Figure 5a shows the agglomerated nano-particles of pure ZnO. In Fig. 5b, c, with Ag doping in ZnO i.e. ZnOAg1 ($x=0.02$) and ZnOAg4 ($x=0.1$) shows decrease

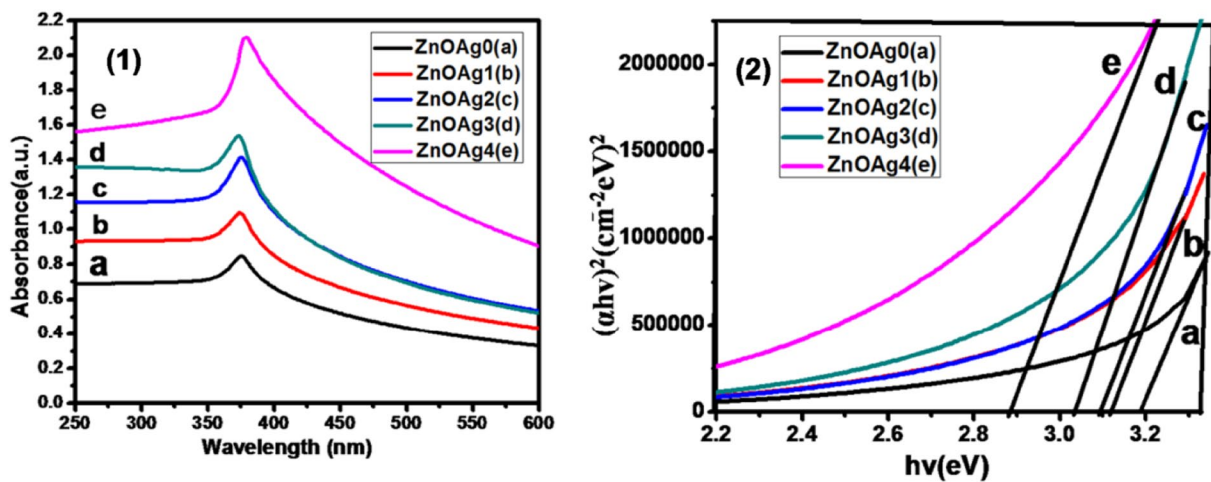
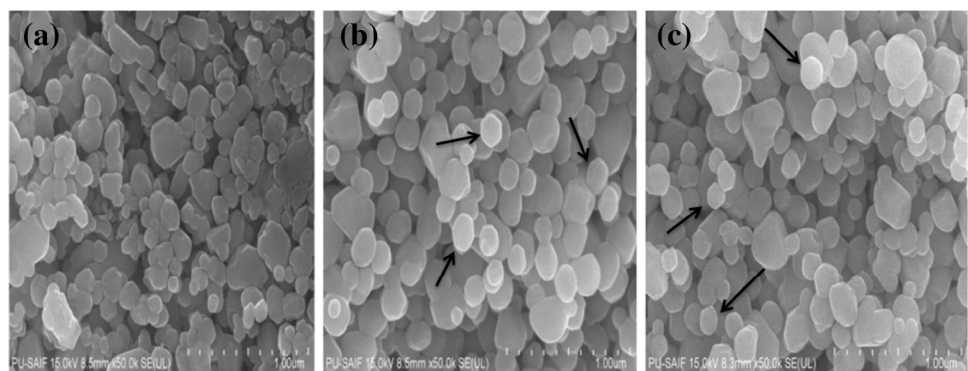


Fig. 4 Left absorption spectra of ZnOAg0, ZnOAg1, ZnOAg2, ZnOAg3, ZnOAg4 and right optical band gap for corresponding absorption patterns

Table 2 The absorption maxima and optical band gap values (E_{opt}) for ZnOAg0, ZnOAg1, ZnOAg2, ZnOAg3 and ZnOAg4 respectively

Name of Sample	ZnOAg0	ZnOAg1	ZnOAg2	ZnOAg3	ZnOAg4
Absorption maxima (nm)	373.2	374.2	374.5	374.9	377
Optical band gap (eV) E_{opt}	3.13	3.07	2.98	2.88	2.75

Fig. 5 FESEM images. a ZnOAg0, b ZnOAg1, c ZnOAg4



in agglomeration of nano-particles due to doping of silver. In addition to this, doping of silver into ZnO will also lead to give regular shape to final NPs as compare to pure ZnO NPs as shown in Fig. 5b, c by arrow marks. Least agglomeration and regular organization of Ag doped ZnO based final NPs can lead to new outcomes in dye degradation application.

3.5 EDAX and mapping study

EDAX spectrum of ZnOAg0 (a) and ZnOAg4 (b) are shown in Fig. 6. In Fig. 6a, presence of zinc (Zn), oxygen (O) elements peaks confirms the purity of ZnO NPs. The presence of silver (Ag) peak in ZnO (ZnOAg4) matrix gives the presence of Ag in ZnO matrix. The intensity of Ag peak depend on the content level of silver in ZnO matrix. Further to confirm the homogeneity of content of synthesized nanoparticles the NPs were analyzed with EDAX in mapping mode whose data is summarized in Fig. 7. This study strongly supports and confirms the Fig. 6 results as the Fig. 7a–c, a1–c1 gives mapping mode based representation of ZnOAg0 and ZnOAg4 respectively.

3.6 TEM study

The morphology of pure ZnO and Ag doped ZnO NPs were observed with Hitachi H-7500 TEM. Images of ZnOAg0, ZnOAg1 and ZnOAg4 are shown in Fig. 8a–c respectively. TEM confirms the monodisperse and uniform particle size of NPs. With Ag doping to pure ZnO NPs, we find clear contrast enhancement in Fig. 8b, c as compare to Fig. 8a.

This clearly confirms the presence of Ag in ZnO matrix which fully supported by EDAX study. In Fig. 8a, b, the particle size decreases from 47 to 46 nm, and then increases to 58 nm in Fig. 8c, which matches with XRD result. The uniform, regular shape of NPs may directly affect the efficiency of nanoparticles in their applications.

3.7 Photo degradation study

The photo degradation efficiency of ZnO and Ag doped ZnO were investigated on methylene blue (MB) and Brilliant blue (BB) dyes. The dye concentration used in reaction was 20 ppm and 25 mg content of different NPs series were added in dye solution for specific reaction time under specific condition. The absorption patterns of different NPs were recorded corresponding to maximum absorption wavelength of MB and BB using UV–Visible Spectroscopy. According to Beer–Lambert law, concentration of dye is proportional to its absorbance, so its % degradation efficiency can be calculated by Eq. 6 [38, 39]

$$R = \frac{C_0 - C}{C_0} \times 100\% = \frac{A_0 - A}{A_0} \times 100\% \quad (6)$$

where C_0 , C , A_0 , A are concentration and absorbance of dye at reaction condition time (0) and (t) minute respectively.

The percentage dye degradation of different NPs are calculated with Eq. 6. All values are summarized in Tables 3 and 4 and their corresponding absorption spectra are shown in Figs. 9 and 10 respectively. Absorption spectra in Fig. 9(left), shows the intensity of diminished MB dye with irradiation time of visible light exposure. The diminishing

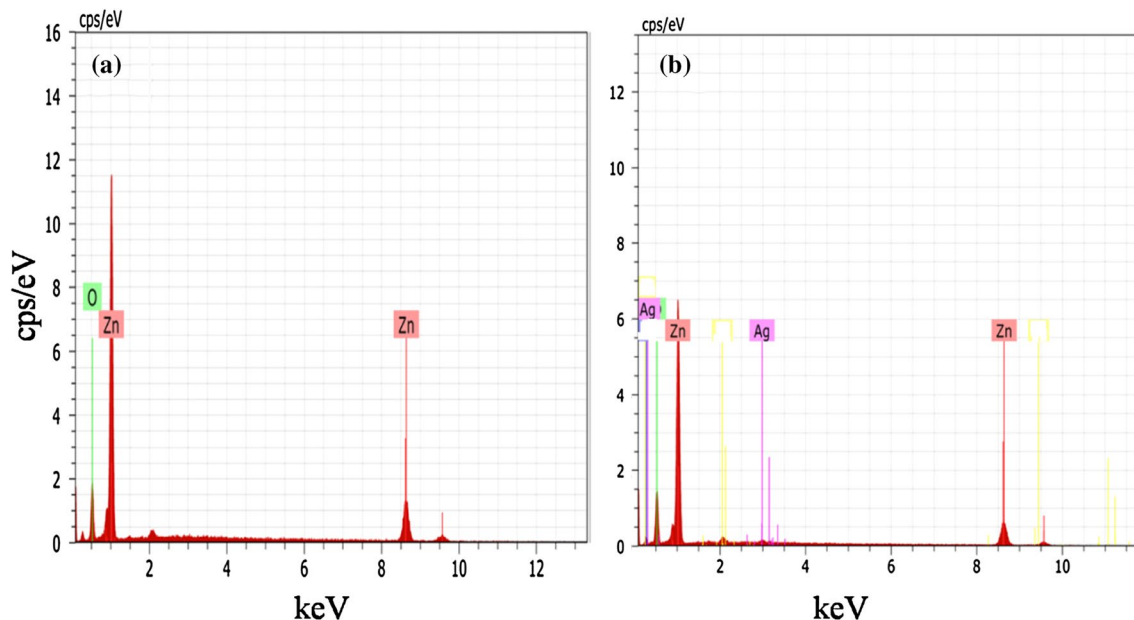


Fig. 6 EDAX spectrum of **a** Pure ZnO (ZnOAg0). **b** Ag doped ZnO (ZnOAg4)

Fig. 7 EDAX mapping *left* ZnOAg0. **a** Mapped area, **b** zinc, **c** oxygen and *right* ZnOAg4. **a1** Mapped area, **b1** zinc, **c1** oxygen, **d1** silver respectively

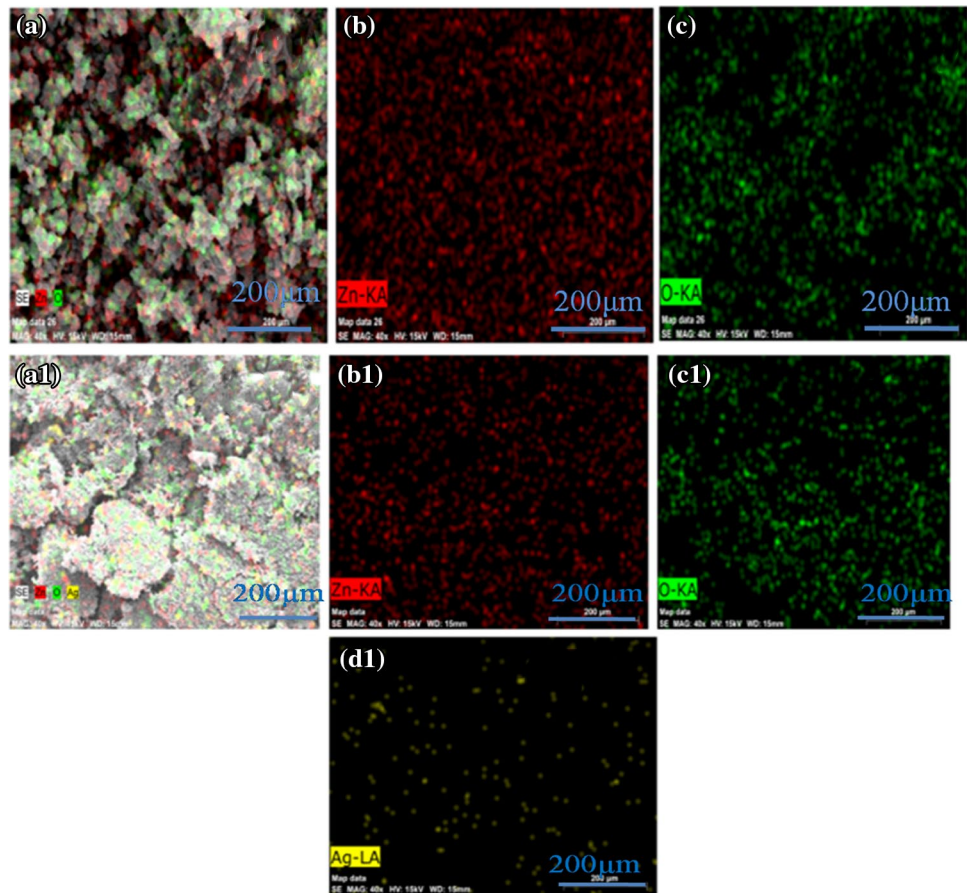
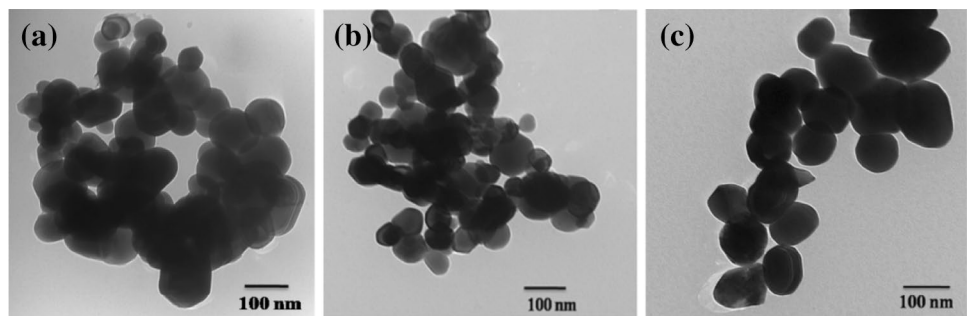


Fig. 8 TEM images. **a** ZnOAg0, **b** ZnOAg1, **c** ZnOAg4 respectively



effect of absorbance (at wavelength maxima ~662 nm) of MB was pronounced after 80 min exposure time of NPs with dye. The percentage MB degradation efficiency of pure ZnO and different concentration of Ag (X=0.02, 0.04, 0.06, 0.1) in ZnO rises from 41.55 to 96.78%, 43.70 to 97.59, 44.24 to 97.72, 44.77 to 97.83 and 45.58 to 98.66 for 20–180 min irradiation time respectively. In continuation the degradation efficiency (at wavelength maxima ~550 nm) of BB under same condition shown in Fig. 10 (percentage BB dye degradation rises from 17.95 to 82.15, 32.76 to 94.12, 58.62 to 95.23, 59.43 to 94.62 and 55.38 to 97.36 for same series). BB shows drastic increase after 20 min irradiation time exposure (~20% degradation) which

are summarized in Table 4, whose reason mention in degradation mechanism study. Further on comparing MB and BB degradation behavior in Table 4, MB % degradation rises to ~30% from 80 to 120 min irradiation time exposure whereas BB rises to only ~5%. which is an effort to explore mechanism part of dye degradation. The saturation of percentage dye degradation values for MB and BB at 180 min irradiation time can be due to agglomeration of NPs, which lead to violate the generation of electron/hole theory [40, 41]. Due to agglomeration of ZnO NPs may lead to short circuiting the reaction without generating active species retard the reaction and leads to non availability of proper sites for further creation mechanism of electron/hole ion

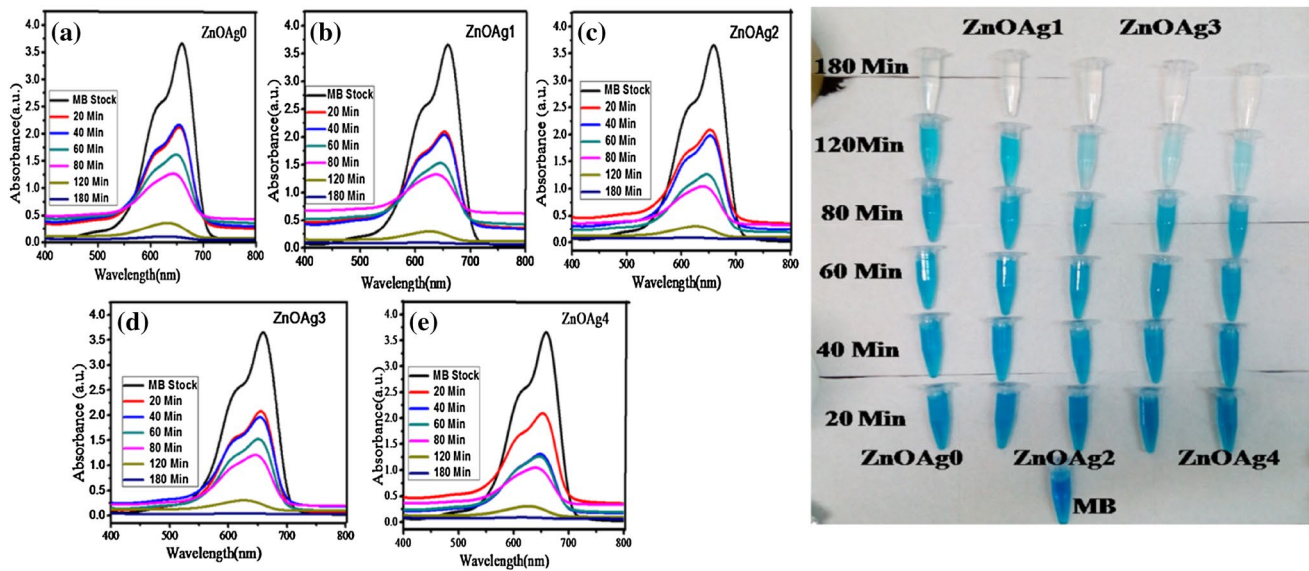


Fig. 9 Left absorption spectral changes of MB with **a** ZnOAg0, **b** ZnOAg1, **c** ZnOAg2, **d** ZnOAg3, **e** ZnOAg4. Right physical appearance of different samples at different timings respectively

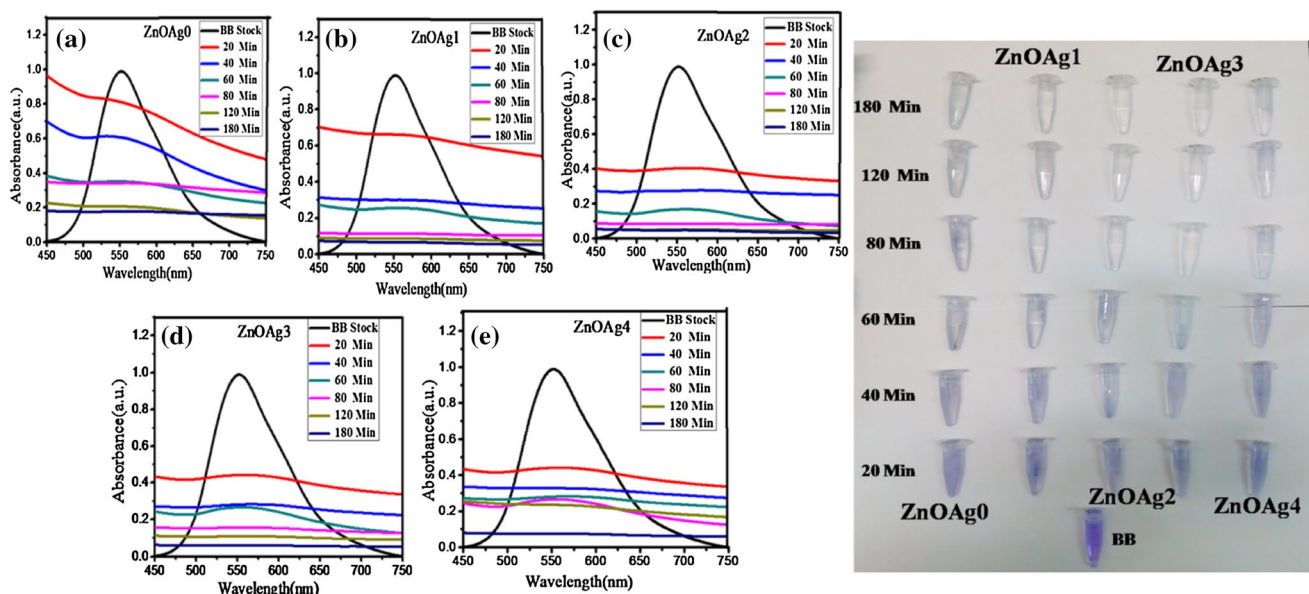


Fig. 10 Left absorption spectral changes of BB with **a** ZnOAg0, **b** ZnOAg1, **c** ZnOAg2, **d** ZnOAg3, **e** ZnOAg4. Right physical appearance of different samples at different timings respectively

[42]. In addition with increasing content of silver to ZnO may lead to give localized cluster which makes inhomogeneous distribution leads to reduction of surface availability for adsorption of light and reactant [43].

As Ag doping in ZnO increases from $Zn_{1-x}OAg_x$, $x=0$ to 0.1 M, a decrease in optical band gap from 3.13 to 2.75 eV is observed, which directly lead to more absorption of visible light and more efficiently transfer of photo generated electron from excited dye to ZnO surface through Ag

NPs. This leads to higher dye degradation [44]. The Ag^+ in ZnO captures the photo induced electron which further act as electron trap and decrease the recombination of electron-hole. On basis of availability of charge carriers will lead to generate more reactive oxygen sites (ROS) which further break and degrade the dye into degraded product. In contrast of XRD (crystallite size) and TEM (particle size) study, the increased dye degradation behavior with increased crystallite size and particle size of ZnO NPs can

be possibly due to their increase crystallinity. The increase in crystallinity of Ag doped ZnO NPs can be confirmed with decrease in FWHM value for 101 peak were shown in Table 1[45]. The increased crystallinity of ZnO NPs may possibly lead to reduction of capturing of electron by different defect sites resulting in high efficiency of electron transfer in bulk NPs [46]. Different defects in Ag-ZnO broadly includes-singly ionized oxygen, oxygen antisite, zinc vacancy etc [47].

In continuation, Fig. 11a, b shows the pictorial representation of percentage dye degradation data for MB and BB dye respectively. The photo catalytic activity of MB and BB with ZnO NPs was also checked under dark environment to find the effect of adsorption. MB and BB does not show prominent effect due to adsorption in photo catalytic reaction.

The increased MB percentage degradation by NPs with time is also related with rate constant for different samples and can be described by following kinetic model [48]:

$$Rate = -\frac{dC}{dt} = \frac{kKC}{1 + KC} \tag{7}$$

where C is concentration of dye (mg/L) at any time t, t is irradiation time, k is first order constant of reaction and K is adsorption constant of pollutant on NPs. Further this equation can be simplified to pseudo-first-order-equation [49]:

$$Ln\left(\frac{C}{C_0}\right) = -k_{obs}t = k_{obs}t \tag{8}$$

where k_{obs} is observed first order rate constant of reaction.

The first order rate constant for degradation reaction (k_{obs}) of MB and BB were calculated by plot of $Ln(C/C_0)$ versus irradiation time for different ZnO NPs in Fig. 12a,

b and inset figure gives their corresponding linear fit. In Fig. 12a k_{obs} , for MB increases from 0.022, 0.023, 0.023, 0.024 and 0.026 and BB from 0.013, 0.017, 0.017, 0.018 and 0.019 for pure ZnO and different concentration of Ag (X=0.02, 0.04, 0.06, 0.1) in ZnO respectively. High rate constant for catalyst with MB (0.022–0.026/min) as compare to BB (0.013–0.019/min) have justify the higher % removal of MB as compare to BB. Rate constant values for NPs catalyst for MB and BB were summarized in Tables 3 and 4.

3.8 Mechanism of photo-catalytic reaction

The degradation behavior of dye (MB and BB) under visible light irradiation can have two possible mechanisms. One is ability of ZnO based photo catalyst to generate electron-hole pair. In presence of oxygen defects or metal nanoparticles on ZnO NPs surface leads to enhancement of the separation of photo generated electron-hole pair [50] which are major factor for color fading of dye. Other mechanism is based on excitation of dye in which dye act as the sensitizer will transfer electron to electron acceptor sites and itself becomes cationic free radical. Unstable dye will further lead to self degradation or degradation by oxidizing species, as shown in Fig. 13(right).

When ZnO NPs are exposed to visible light the electron-hole are generated, the electron from the conduction band and hole from valance band, separate on the surface of catalyst. The photoexcited electron may lead to produce super oxide anion radical O_2^- which further generate H_2O_2 and OH. Radicals [51]. Hole leads to creating reactive hydroxyl group through water. The oxygen vacancies act as traps for photoinduced electrons which further restrain temporarily the recombination of photogenerated

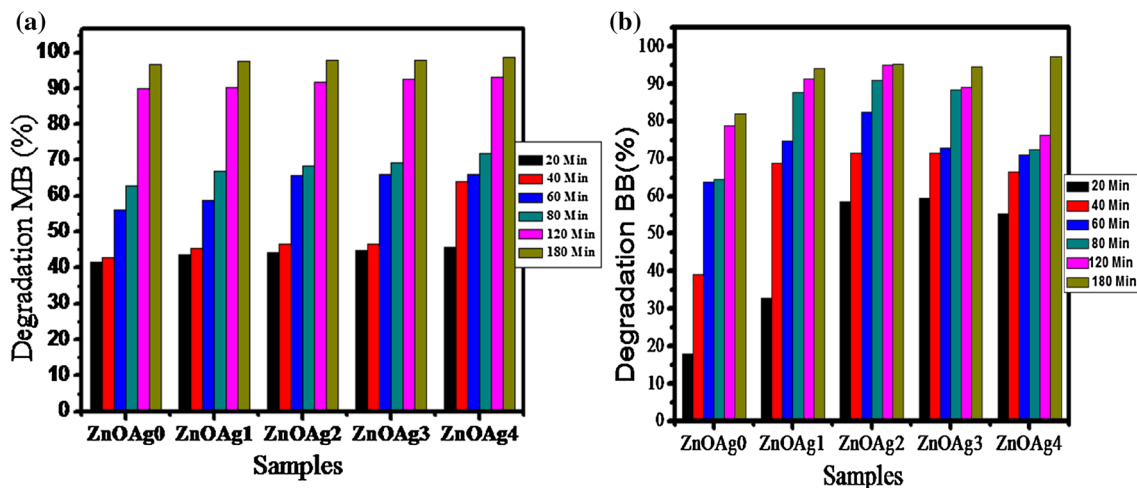


Fig. 11 a, b Pictorial representation of % dye removal for MB and BB dye respectively

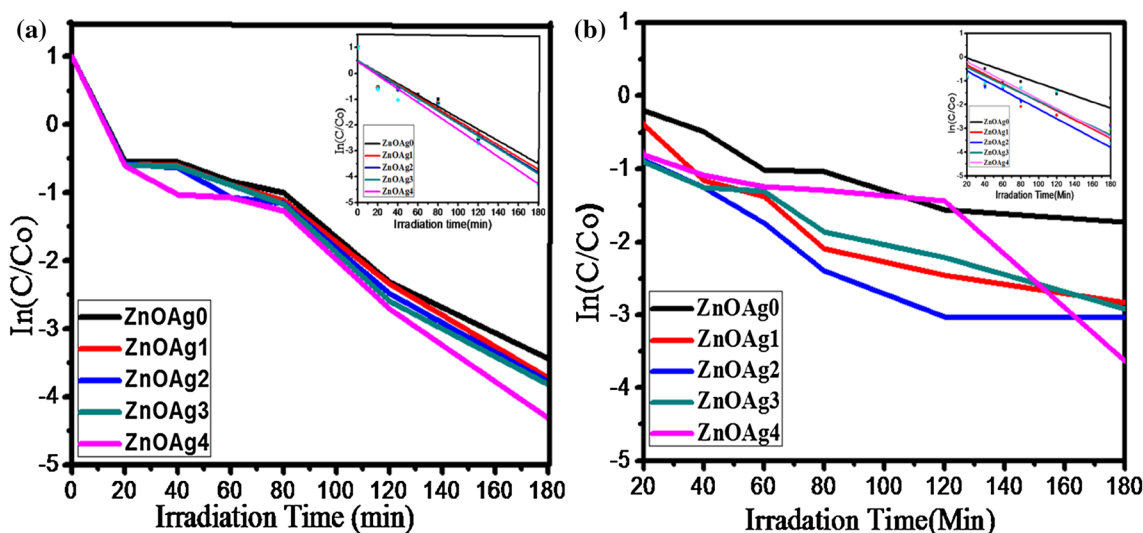


Fig. 12 a, b Plots of Ln (C/Co) versus irradiation time for photo degradation of MB and BB in presence of ZnOAg0, ZnOAg1, ZnOAg2, ZnOAg3 and ZnOAg4 under visible light (Inset figures gives corresponding linear fit)

Table 3 % Dye degradation of MB with ZnOAg0, ZnOAg1, ZnOAg2, ZnOAg3, ZnOAg4 with irradiation time and their corresponding rate constant respectively

Name of sample	Irradiation time (min)						Rate constant (min ⁻¹)
	20 min	40 min	60 min	80 min	120 min	180 min	
Degradation efficiency (%) for MB							
ZnOAg0	41.55	42.63	56.30	63.00	90.08	96.78	0.022
ZnOAg1	43.70	45.31	58.71	67.02	90.35	97.59	0.023
ZnOAg2	44.24	46.65	65.68	68.36	91.69	97.72	0.023
ZnOAg3	44.77	46.54	58.98	69.17	92.49	97.83	0.024
ZnOAg4	45.58	64.08	65.95	71.85	93.30	98.66	0.026

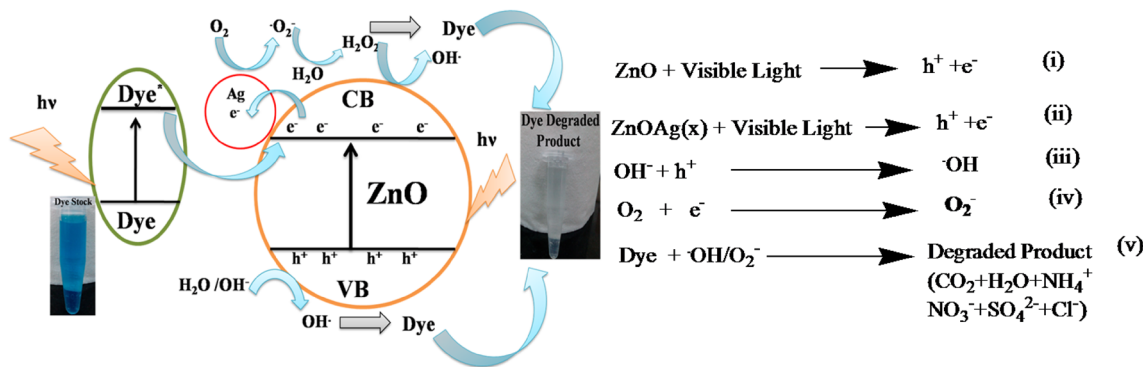


Fig. 13 Left schematic representation of dye degradation in presence of ZnO NPs (catalyst). Right proposed photo-catalytic reaction mechanism for same

electron–hole. The photogenerated electron further attack the dissolved oxygen and create surface bound superoxide anion along with hydroxyl ion which is further responsible for dye mineralization for photocatalytic reaction [52].

The generated OH· radical is enough to break the different bond in the dye (C–N, C=N, C–S, N=N, C–C etc) and lead to convert dye into CO₂ and inorganic ions (NH₄⁺, NO₃⁻, SO₄²⁻ etc). The irradiation leads to formation of

more O_2^- and OH. radicals which further degrade the dye completely.

On the basis of mechanism depicted in Fig. 13, following outcomes can be concluded (1) ZnO NPs serve as a source of electron and hole for dye degradation process under irradiation of visible light (Eq. i); (2) Dye can also acts as the source of electron under for ZnO as excitation by visible light leads to transfer delocalized π electron to CB of ZnO, which enriches electron density in ZnO (Fig. 13 schematic diagram); (3) the oxygen vacancy defects (see Eq. iv) and Ag NPs on ZnO surface act as sink for electrons (shown in schematic diagram Fig. 13). Oxygen vacancy defects and Ag on ZnO surface acts as the traps for electron and prevent the recombination of electron–hole pair. (4) the photo induced hole may be easily trapped by OH^- and converted into hydroxyl radical ($\cdot OH$) (Eq. iii); (5) the generated photo induced electron may be trapped by electron acceptor species like adsorbed O_2 leads to form super oxide radical anion (O_2^-) (Eq. iv); (6) finally generated hydroxyl radical ($\cdot OH$) and super oxide radical anion (O_2^-) may have significant role in overall photo catalytic reaction (Eq. v). In diagram Fig. 13, we have found the colored and decolorized dye before and after photo catalytic reaction follow the predicted mechanism of dye degradation [53]. Overall, all these facilitation of dye degradation mechanism of MB and BB, are only possible through structural, optical and morphological tuning of Ag incorporation in ZnO matrix.

3.9 Comparison of degradation ability between MB and BB

The factor responsible for the color of any dye broadly depend on chromophore group present in its structure. MB and BB differ in their molecular structure, functional group and extent of ionization in aqueous solution. Due to common basic nature (cationic) of both dyes, the rest factor i.e. functional group and extent of ionization will decide the result. Degradation ability of MB and BB dye with ZnO NPs correlated with number of chromophoric sites and their destabilization through free radical generation by photo catalysis reaction. In Fig. 14(left), MB structure has four possible chromophoric site present (shown by arrow) and four methyl group (shown by box) whereas in BB (left) has seven active sites (shown by arrow) for the photo-catalytic reaction. Attacking species generated in ZnO NPs ($\cdot OH$ or O_2^- etc) under visible light (shown in Fig. 13), lead to break or destabilize the present chromophoric sites [54] in dye (MB or BB). On comparison of degradation of MB and BB, MB has additionally four methyl group having + Inductive effect, which further protect the dye from destabilization. This explanation can be directly correlated with slow MB degradation from 20 to 40 min (Table 3) as compare to BB degradation in same irradiation time (Table 4) respectively. Further from 80 to 120 min irradiation time exposure, MB dye leads to drastically enhanced

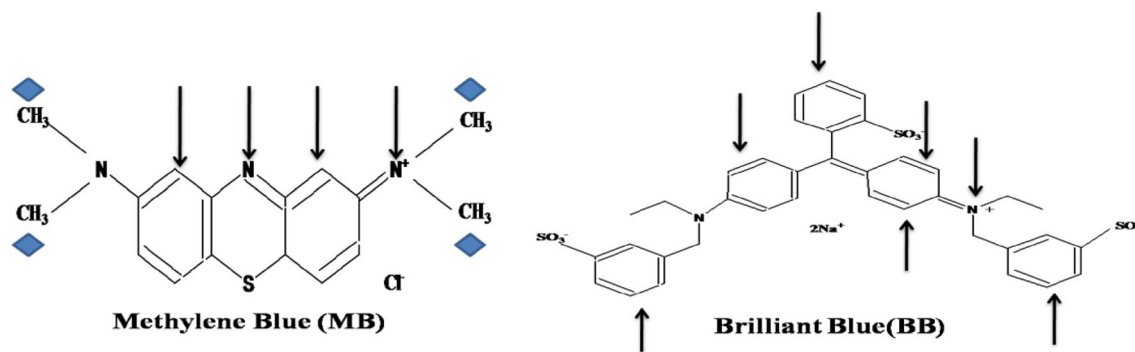


Fig. 14 Left structure of methylene blue dye (MB). Right brilliant blue respectively

Table 4 % Dye degradation of BB with ZnOAg0,ZnOAg1,ZnOAg2, ZnOAg3, ZnOAg4 with irradiation time and their corresponding rate constant respectively

Name of sample	Irradiation time (min)						Rate constant (min^{-1})
	20 min	40 min	60 min	80 min	120 min	180 min	
Degradation efficiency (%) for BB							
ZnOAg0	17.95	39.15	63.69	64.50	78.90	82.15	0.013
ZnOAg1	32.76	68.76	74.75	87.63	91.38	94.12	0.017
ZnOAg2	58.62	71.50	82.56	90.87	95.13	95.23	0.017
ZnOAg3	59.43	71.60	72.92	88.48	89.08	94.62	0.018
ZnOAg4	55.38	66.43	71.10	72.41	76.41	97.36	0.019

the % degradation (~20%) as compare to BB dye (~10%). This may be possibly due to prominent effect of incident energy (enriches with oxidizing species responsible to degradation) for MB dye to break or destabilize its structure as compared to BB. Finally both dye after 180 min irradiation exposure, leads to degrade 41.55–96.78, 45.58–98.66 and 17.95–82.15, 55.38–97.36 after 20–180 min exposure for ZnOAg0 and ZnOAg4 respectively. Conclusively from above study MB degradation efficiency is more as compare to BB in presence of Ag doped ZnO. This can be possibly due to reason that MB dye has less chromophoric site as compared to BB dye.

4 Conclusion

Ag doped ZnO modified NPs were synthesized under co-precipitation method. XRD study confirmed the structural purity of ZnO NPs. In XRD the calculated crystallite size increases from 46.67 to 54.80 nm, lattice strain changes from 23.90 to 22.36×10^{-4} with respect to pure ZnO and different Ag doped ZnO NPs respectively. XRD, EDAX and UV–Vis study clearly confirms the presence of Ag in ZnO matrix. TEM and FESEM have given morphological quality of synthesized nanoparticles. The heterogeneous degradation efficiencies of ZnO semiconductor NPs under visible light irradiation are enhanced by co-precipitation synthesis method and silver (Ag) doping into ZnO matrix. The % MB, BB dye degradation rises from 41.55 to 96.78, 43.70 to 97.59, 44.24 to 97.72, 44.77 to 97.83 and 45.58 to 98.66 and 17.95 to 82.15, 32.76 to 94.12, 58.62 to 95.23, 59.43 to 94.62 and 55.38 to 97.36% for ZnOAg0, ZnOAg1, ZnOAg2, ZnOAg3 and ZnOAg4 respectively. Final MB dye degradation efficiency is high as compared to BB dye which is confirmed by high rate constant of MB (0.022–0.026) as compared to BB degradation rate constant (0.013–0.019) respectively. Although initially MB dye degradation proceed slowly as compared to BB dye due to presence of +I effect sites ($-\text{CH}_3$ group) in MB structure which resist the structure from destabilization by oxidizing agent in photo catalysis. As the exposure time of visible light with NPs increases, MB dye structure get destabilize through chromophoric site (only four site) as compare to BB dye (having seven site). Due to less chromophore site in MB as compare to BB dye will bring effective and efficient dye degradation ability of MB with NPs. The co-precipitation based induced Ag /ZnO photo catalyst in this work proposes one of effective and efficient candidate to treat the polluted water from textile industry and other organic pollutant of water under visible light irradiation.

Acknowledgements The author would like to thank SAIF, Panjab University Chandigarh for providing characterization facilities.

References

1. N. Kislov, J. Lahiri, Himanshu Verma, D.Y. Goswami, E. Stefanos, M. Batzill, Photocatalytic degradation of Methylene Orange over single crystalline ZnO: Orientation dependence of Photoactivity and photostability of ZnO. *Langmuir* **25**, 3310–3315 (2009)
2. R.R. Bhosale, S.R. Pujari, G.G. Muley, S.H. Patil, K.R. Patil, M.F. Shaikh, A.B. Gambhire, Solar photocatalytic degradation of methylene blue using doped TiO₂ nanoparticles. *Sol. Energy* **103**, 473–479 (2014)
3. K.M. Parida, S. Parija Photocatalytic degradation of phenol under solar radiation using microwave irradiated zinc oxide. *Sol. Energy*, **80**, 1048–1054 (2006)
4. M. Sharma, T. Sharma, S. Singh, O.P. Pandey, Photocatalytic degradation of organic dyes under UV–Visible light using capped ZnS nanoparticles. *Sol. Energy* **86**, 626–633 (2012)
5. D.W. Hwang, J. Kim, T.J. Park, J.S. Lee, Mg-doped WO₃ as a novel photocatalyst for visible light-induced water splitting. *Catal. Lett.* **80**, 53–57 (2002)
6. F. Chen, Y. Cao, D. Jia, X. Niu, Facile synthesis of CdS nanoparticles photocatalyst with high performance. *Ceram Int.* **39**, 1511–1517 (2013)
7. Y.K. Mishra, V.S.K. Chakravadhanula, V. Hrkac, S. Jebril, D.C. Agarwal, Crystal growth behavior in Au–ZnO nanocomposite under different annealing environment and photoswitchability. *J. Appl. Phys.* **112**, 64308 (2012)
8. T. Ootsuka, Z. Liu, M. Osamura, Y. Fukuzawa, R. Kuroda, Y. Suzuki, N. Otagawa, T. Mise, S. Wang, Y. Hoshino, Y. Nakayama, H. Tanoue, Y. Makita, Studies of Aluminium-doped ZnO films for transparent electrode and anti reflection coating of β -FeSi₂ optoelectronic devices. *Thin Solid Films* **476**, 30–34 (2005)
9. A. Dongmin, Li. Yan, Li. Xiaoxue, Z. Yunling, D. Guozhi, Synthesis of porous of ZnO structure for gas sensor and photocatalytic applications. *Colloids Surf. A Physicochem. Eng. Asp.* **447**, 81–87 (2014)
10. M. Krayaoui, A. Mhamdi, H. Kaouach Labidi, A. Boukha-chem, K. Boubaker, M. Amlouk, R. Choturou, Some physical investigation on silver–ZnO doped sprayed thin films. *Mat. Sci. Semicon. Proc.* **30**, 255–262 (2015)
11. J.M. Szarko, J.K. Song, C.W. Blackledge, I. Swart, S.R. Leone, S. Li, Y. Zhao, Optical injection probing of single ZnO tetrapod lasers. *Chem. Phys. Lett.* **404**, 171–176 (2005)
12. H. Yin, P.S. Casey, ZnO nanorod composite with quenched photoactivity for UV protection application. *Mater. Lett.* **121**, 8–11 (2014)
13. P. Liu, Y. Guo, Q. Xu, F. Wang, Y. Li, K. Shao, Enhanced photocatalytic performance of ZnO/multi-walled carbon nanotube nanocomposites for dye degradation. *Ceram. Int.* **40** 5629–5633 (2014)
14. S. Ekamparam, Y. Iikubo, A. Kudo, Combustion synthesis and photocatalytic properties of transition metal-incorporated ZnO. *J. Alloy. Compd* **433**, 237–240 (2007)
15. R. Wang, J.H. Xin, Y. Yang, H. Liu, L. Xu, J. Hu, The characteristics and photocatalytic activities of silver doped ZnO nanocrystallites. *Appl. Surf. Sci.* **227**, 312–317 (2004)
16. Q.H. Li, Y.X. Liang, Q. Wan, T.H. Wang, Oxygen sensing characteristics of individual ZnO nanowire transistor. *Appl. Phys. Lett.* **85**, 6389–6391 (2004)
17. A.K. Gouvea, F. Wypych, S.G. Moraes, N. Duran, N. Nagata, P. Peralta-Zamora, Semiconductor-assisted photocatalytic degradation of reactive dyes in aqueous solution. *Chemosphere* **40**, 433–440 (2000)

18. J. Liqiang, W. Baiqi, X. Baifu, L. Shudan, S. Keying, C. Weimin, F. Honggang, Investigations on the surface modification of ZnO photocatalyst by depositing Pd. *J. Solid State Chem* **177**, 4221–4227 (2004)
19. O.D. Jayakumar, H.G. Salunke, R.M. Kadam, M. Mohapatra, G. Yaswant, S.K. Kulshreshtha, *Nanotechnology* **17**, 1275–1278 (2006)
20. V. Gandhi, H.H.A. R. Ganesan, Sayedhamed, M. Thaiyan, Effect of cobalt doping on structure, optical, and magnetic properties of ZnO nanoparticles synthesized by Coprecipitation method. *J. Phys. Chem. C* **118**, 9715–9725 (2014)
21. J.J. Wu, C.H. Tseng, Photocatalytic properties of nc-Au/ZnO nanorods composites. *Appl. Catal. B* **66**, 51–57 (2006)
22. M. K. Seery, R. George, P. Floris, and S. C. Pillai, Silver doped titanium oxide nanomaterials for enhanced visible light photocatalysis. *J. Photochem. Photobiol. A* **189**, 258–263 (2007)
23. Y. Zheng, L. Zheng, Y. Zhan, X. Lin, Q. Zheng, K. Wei, Ag/ZnO heterostructure nanocrystals: synthesis, characterization, and photocatalysis. *Inorg. Chem* **46**, 6980–6986 (2007)
24. C. Karunakaran, V. Rajeswari, and P. Gomathisankar, Enhanced photocatalytic and antibacterial activities of sol–gel Synthesized ZnO and Ag-ZnO. *Mater. Sci. Semicond. Process.* **14**, 133–138 (2011)
25. R. Ullah, J. Dutta, Photocatalytic degradation of organic dyes with manganese-doped ZnO nanoparticles. *J. Hazard. Mater.* **156**, 194–200 (2008)
26. C.A.K. Gouvea, F. Wypych, S.G. Moraes, N. Duran, P.P. Zamora, *Chemosphere* **40**, 427–432 (2000)
27. C. Karunakaran, V. Rajeswari, P. Gomathisankar, Antibacterial and photocatalytic activities of sonochemically prepared ZnO and Ag-ZnO. *J. Alloys Compd.* **508**, 587–591 (2010)
28. B. Subash, B. Krishnakumar, R. Velmurugan, M. Swaminathan, M. Shanthi, Synthesis of Ce co-doped Ag-ZnO photocatalyst with excellent performance for NBB dye degradation under natural sunlight illumination. *Catal. Sci. Technol.* **2**, 2319–2326 (2012)
29. R. Georgekutty, M.K. Seery, S.C. Pillai, A highly efficient Ag-ZnO photocatalyst: synthesis, properties, and Mechanism. *J. Phys. Chem. C* **112**, 13563–13570 (2008)
30. V. Vamathevan, R. Amal, D. Beydoun, G. Low, S. McEvoy, Photocatalytic oxidation of organics in water using pure and silver-modified titanium oxide particles. *J. Photochem. Photobiol. A* **148**, 233 (2002)
31. C. Karunakaran, V. Rajeswari, P. Gomathisankar, Antibacterial and photocatalytic activities of sonochemically prepared ZnO and Ag-ZnO. *J. Alloy. Compd* **508**, 587–591 (2010)
32. R.S. Zeferino, M.B. Flores, U. Pal, Photoluminescence and Raman scattering in Ag-doped ZnO nanoparticles. *J. Appl. Phys.* **109**, 014308 (2011)
33. S.S. Lin, J.L. Huang, D.F. Lii, Effect of substrate temperature on the properties of TiO₂ doped ZnO films by simultaneous rf and dc magnetron sputtering. *Mater. Chem. Phys.* **90**, 22–30 (2005)
34. P.P. Sahay, R.K. Nath, Al -doped ZnO thin films as methanol sensor. *Sens. Actuators B* **134**, 654–659 (2008)
35. Y. Jin, Q. Cui, K. Wang, J. Hao, Q. Wang, J. Zhang, Investigation of photoluminescence in undoped and Ag-doped ZnO flowerlike nanocrystal. *J. Appl. Phys.* **109** (5), 053521 (2011)
36. H. Lv, D.D. Sang, H.D. Li, X.B. Du, D.M. Li, G.T. Zou, Thermal evaporation synthesis and properties nano/microstructure using carbon group elements as the reducing agents. *Nanoscale Res. Lett* **5**, 620–624 (2010)
37. Y. Ramadin, M.A.H. Abdallah, M. Ahmad, A. Zihilif, S.K.J.A. Ani, S.G.K.A. Ani, Optical properties of epoxy-glass micobalons composite. *Optical materials* **5**, 69–73 (1996)
38. K. Wang, L. Yu, S. Yin, H. Li, H. Li, Photocatalytic degradation of methylene blue on magnetically separable FePc/Fe₃O₄ nanocomposite under visible irradiation. *Pure Appl. Chem.* **81**, 2327–2335 (2009)
39. Y. Abdollahi, A.H. Abdullah, Z. Zainal, N.A. Yusof, Photocatalytic degradation of p-cresol by Zinc oxide under UV irradiation. *Int. J. Mol. Sci.* **13**, 302–315 (2012)
40. B. Li, H. Cao, ZnO@ Graphene composite with enhanced performance for the removal of dye from water. *J. Mater. Chem* **21**, 3346–3349 (2011)
41. S.M. Toress, L.M.P. Martinez, J.L. Figueiredo, J.L. Faria, A.M.T. Silva, Graphene oxide P-25 photocatalyst for degradation of diphenhydramine pharmaceutical and methylene orange dye. *Appl. Surf. Sci* **275**, 361–378 (2013)
42. I.K. Konstantinou, T.A. Albanis, TiO₂-assisted photocatalytic degradation of azo dyes in aqueous solution: kinetic and mechanistic investigation: a review. *Appl. Catal. B-Environ.* **49**, 1–14 (2004)
43. R. Georgekutty, M.K. Seery, S.C. Pillai, A highly efficient Ag-ZnO photocatalyst: synthesis, properties and mechanism. *J. Phys. Chem.* **112**, 13563–13570 (2008)
44. Y.J. Jang, C. Simer, T. Ohm, Comparison of zinc oxide nanoparticles and its nano-crystalline particle on the photocatalytic degradation of methylene blue. *Mater. Res. Bull.* **41**, 67–77 (2006)
45. J.Z. Kong, A.D. Li, X.Y. Li, H.F. Zhai, W.Q. Zhang, Y.P. Gong, H. Li, D. Wu, Photo degradation of methylene blue using Ta-doped ZnO nanoparticle. *J. Solid State Chem.* **183**, 1359–1364 (2010)
46. V. Taghvaei, A.H. Yangjeh, M. Behboudnia, Hydrothermal and template-free preparation and characterization of nanocrystalline ZnS in presence of low-cost ionic liquid and photocatalytic activity. *Physica E* **42**, 1973–1978 (2010)
47. Y. Zheng, L. Zheng, Y. Zhan, X. Lin, Q. Zheng, K. Wei, Ag/ZnO heterostructure nanocrystal: synthesis, characterization and photocatalysis. *Inorg. Chem.* **46**, 6980–6986 (2007)
48. X. Xu, R. Lu, X. Zao, S. Xu, X. Lei, F. Zhang, D.G. Evans, Fabrication and photocatalytic performance of Zn_xCd_{1-x} S solid solution prepared by sulfuration of a single layered double hydroxide precursor. *Appl. Catal. B.* **102**, 147–156 (2011)
49. A. Wood, M. Giesig, P. Mulvaney, Fermi level equilibration in quantum dot-metal nanojunctions. *J. Phys. Chem* **105**, 8810–8815 (2001)
50. C.A.K. Gouvea, F. Wypych, S. Moraes, N. Duran, N. Nagata, P.P. Zamora, Semiconductor-assisted photocatalytic degradation of reactive dyes in aqueous solution. *Chemosphere* **40**, 433–440 (2000)
51. V. Kandavelu, H. Kastien, K.R. Thampi, Photocatalytic degradation of isothiazolin-3-ones in water and emulsion paints containing nanocrystalline TiO₂ and ZnO catalyst. *Appl. Catal. B* **48**, 101–111 (2004)
52. G. Merci, V. Augugliaro, M.J.L. Munoz, C. Martin, L. Palmisano, V. Rives, M. Schiavello, R.J.D. Tillley, A.N. Venezia, Preparation characterization and photocatalytic activity of polycrystalline ZnO/TiO₂ System.2. Surface, bulk characterization, and 4-Nitrophenol photodegradation in liquid–solid regime. *J. Phys. Chem.* **105**, 1033–1040 (2001)
53. H. Yatmaz, A. Akyol, M. Bayramoglu, Kinetics of photocatalytic decolorization of an Azo reactive dyes in aqueous ZnO suspensions. *Ind. Eng. Chem. Res.* **43**, 6035–6039 (2004)
54. A. R. Kataee, M. B. Kasiri, Photocatalytic degradation of organic dyes in the presence of nanostructured titanium dioxide: Influence of chemical structure of dye. *J. Mol. Catal. A-Chem.* **328**, 8–26 (2010)